

Catalytic Reduction of Nitrous Oxide by the Low-Symmetry Pt₈ Cluster

Erendida Hernández,[†] Virineya Bertin,[†] Jorge Soto,[‡] Alan Miralrio,[§] and Miguel Castro^{*,§}

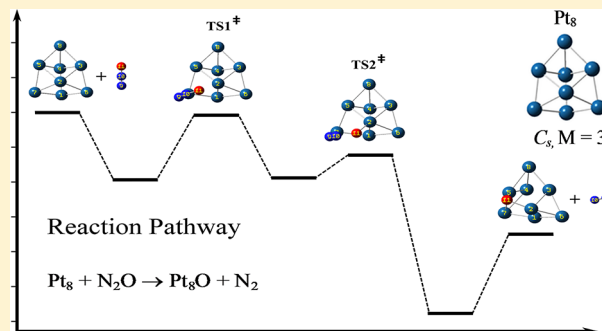
[†]Departamento de Química, Universidad Autónoma Metropolitana-Iztapalapa, San Rafael Atlixco 186, Col. Vicentina, México, D.F. 09340, Mexico

[‡]Departamento de Física, Facultad de Ciencias, Universidad Nacional Autónoma de México (UNAM), Del. Coyoacán, 04510 México D.F., Mexico

[§]Departamento de Física y Química Teórica, DEPg, Facultad de Química, Universidad Nacional Autónoma de México (UNAM), Del. Coyoacán, 04510 México D.F., Mexico

Supporting Information

ABSTRACT: The search for a catalyst for the reduction of nitrous oxide (N₂O) is now imperative, as this molecule is a very dangerous pollutant. We found that the low-symmetry Pt₈ cluster presents multiple reaction pathways for N₂O rupture, which are regioselective. This result was revealed by means of density functional theory calculations within the zero-order-regular approximation, ZORA, explicitly including relativistic effects. It is further proved that Pt₈ is a competitive N₂O catalyst compared to sub-nanometric rhodium clusters, obtaining similar reaction barriers. The hot adsorption site, a tip atom of Pt₈, and the rotation of the N₂O molecule over the metallic cluster promote the formation of a frustrated bridge activated transition state, Pt₈–N₂O. This transition structure yields to spontaneous dissociation of N₂O without bridge formation. Along this catalytic process, rearrangements within the metal cluster take place, preserving its stability. Moreover, in addition to being important attributes of the Pt₈ particle in the N₂O reduction, fluxionality and multiple reaction pathways may also prevent poisoning effects. Overall, this differs from reported results for more symmetric metal particles also used as catalysts.



1. INTRODUCTION

Presently there is intense research being performed on the catalytic reduction of the nitrous oxide species, NO_x. Many experimental works have revealed that such reduction is usually incomplete, producing the N₂O molecule. In this regard, the quantity of N₂O in the troposphere has remained constant for hundreds of years, but with industrial activity it began to seriously increase, ~0.3% per year, because millions of tons are emitted.¹ N₂O plays an important role in chemical reactions that generate photochemical smog and ozone at soil level. In the stratosphere it may destroy the ozone layer as chloro-fluorocarbon species did.² It also adds to acid rain and can contribute to global warming more significantly than the CO₂ molecule.¹ Thus, there is a need to eliminate the N₂O molecule before it becomes a stream in the atmosphere. Small rhodium clusters are the best catalysts to reduce the N₂O molecule, but as rhodium may become scarce at some point, searching for ways to activate other metal particles that are able to reduce N₂O is imperative. Among transition metals, clusters from the platinum group may be promising candidates to accomplish such a task. In fact, platinum is very important in catalysis; for example, it is a crucial constituent of the three-way catalytic converter in cars. However, spectroscopic studies of Pt_n clusters in the gas phase are limited. There is scarce data on their

infrared vibrational spectra, complicating the assignment of the ground-state (GS) geometry of the clusters. Also, their ionization energies and electron affinities have not yet been measured, which imposes some limitations for the characterization of their electronic properties and reactivity behavior. Within the limited experimental information available, that referring to the high magnetic moment measured for the Pt₁₃ cluster supported in a zeolite^{3–5} (0.27–0.65 μ_B/atom) should be highlighted. Those studies were based on monodisperse distributions of the clusters synthesized and are compatible with a high-symmetry icosahedral or cuboctahedral cluster as theoretically predicted. As a matter of fact, size, geometry, and electronic details of the clusters are important factors to consider in catalysis. Another important point is the plethora of isomers that are near in energy, less than 5 kcal/mol, to the GS. Therefore, not only the GS but also some of these isomers, of different geometry and spin multiplicity, could contribute to the catalytic process under the working conditions of the reaction, usually reaching high temperatures.⁶ It may occur that a higher

Received: November 8, 2017

Revised: January 19, 2018

Published: February 13, 2018

energy isomer exhibits a marked catalytic behavior, because of either the geometric details or the electronic structure, or both.

Most prior studies in cluster heterogeneous catalysis have selected small symmetric clusters. An interesting question we can pose is whether small Pt particles are good catalysts regardless of their symmetry. Aside from the capability of the catalytic metal cluster to donate electrons to the adsorbed N_2O molecule, less symmetric Pt clusters, with some atoms presenting low coordination, are expected to be more reactive. Note that such a low-symmetry state of the cluster may not correspond to the GS, though it should be near. The structure of Pt_n nanoparticles has been studied by different authors^{7–21} along with characterization of the activities of Pt_n to react with N_2O and CO molecules.^{22–25} For the GS of the Pt_8 particle, a triple tetragonal pyramid (TTP) form in a triplet state with point group C_3 was determined.¹⁷ This low-symmetry GS structure of Pt_8 was confirmed in the present study as well as by other authors.¹² The objective of this work is to use the Pt_8 particle as a low-symmetry prototype to explore the catalytic reduction of the N_2O molecule.

It should be mentioned that the determination of the GS structure for the Pt_8 cluster is a difficult task. As a matter of fact, in addition to the TTP triplet low-lying state, other studies have obtained a bi-capped triangular prism in quintet spin state for the GS of Pt_8 .^{20,21} As will be discussed below, assignment of the GS and the other low-lying states depends on the chosen method of Density Functional Theory (DFT), on the quality of the basis sets, on the relativistic effects, and on the Jahn–Teller (JT) distortions during the relaxation procedure, among other effects.

By means of mass spectrometry, the reactions of neutral Pt_n ($n = 4–12$) clusters with N_2O and CO in the gas phase were studied.²² It was found that the O atom is adsorbed and N_2 is released, according to the reaction $\text{Pt}_n\text{O}_{m-1} + \text{N}_2\text{O} \rightarrow \text{Pt}_n\text{O}_m + \text{N}_2$, with $m = 1, 2$; similar rate constants are found both for m values. Chemical reactions of single-charged Pt_n^+ and Pt_n^- clusters with N_2O molecules in the gas phase have also been reported.^{23,24} The results show that the cations have larger reactivity than the anions²³ and that neutral Pt_n does not show a special activity with respect to the N_2O reduction,²² giving reaction products like Pt_8O_2 with adsorbed N_2O . Note that the first molecular reduction is very efficient on the Pt_n cluster. Pt/ SiO_2 surfaces and Pt, Pd, Ir, and Ru/alumina systems were also studied for N_2O reduction.²⁶ However, details of how the reduction proceeds on the sites or faces of the Pt_n clusters are still unknown. That is, what is the apt geometry of the Pt_n cluster for the activation and further breaking of N_2O relative to how the energetic (adsorption and activation energies) properties make such a catalytic process feasible. Spectroscopic infrared multiple photon dissociation (IR-MPD) experiments,²⁷ following the sequential absorption of multiple photons, shows that the internal energy of the cluster increases, overcoming the barriers that lead to N_2O reduction on rhodium cluster surfaces. Even more importantly, investigations using this spectroscopic technique can provide valuable details about the complexes formed in the different reaction stages, including the state of the adsorbed molecules, information about its binding site on the cluster, and the degree of bond activation.²⁷ It is expected that such experiments will be useful also for platinum clusters. Here, using DFT techniques, we present a study of N_2O reduction by the Pt_8 cluster. A scan of all possible local minima and transition structures for the $\text{Pt}_8 + \text{N}_2\text{O}$ reactive system was done. Relativistic effects are fundamental in the study of heavy

atoms such as platinum, and in our calculations they were properly considered. In fact, platinum—located one place before gold on the periodic table—falls within the region where the relativistic effects are of paramount importance for the electronic properties.

2. COMPUTATIONAL PROCEDURE

The ADF 2013.01 package²⁸ was employed to carry out the calculations, which are based on the DFT using the Perdew–Burke–Ernzerhof (PBE)²⁹ method that is a generalized gradient approximation (GGA). Scalar relativistic effects, not including spin–orbit coupling, were accounted for in the zeroth-order regular approximation, ZORA.^{30–32} The DFT ZORA is one of the most accurate approaches to the Dirac equation actually used in studies of molecules or clusters having heavy elements. Besides exchange correlation, relativistic effects, as included here for Pt atoms, are crucial to accurately describe transition metal clusters and their reactions. The 1s to 4d orbitals of the Pt atoms were treated in a frozen core way, which is compatible with ZORA. Thus, 32 electrons define the valence space configuration of the Pt atom: $5s^25p^64f^{14}5d^96s^1$. Slater-type orbitals were used and expanded in a triple- ζ basis set with two polarization functions (TZ2P). All electrons were included for the O and N atoms. The structure of the Pt_8 cluster was optimized for $M = 1, 3, 5, 7$, and 9 spin multiplicities ($M = 2S + 1$, where S is the total spin) to search its GS. During the relaxation procedure, JT symmetry breaking is taken into account by means of all possible subgroups of the highest symmetry point group for the different isomers of the Pt_8 particle. The PBE-ZORA GS located for Pt_8 was selected to study the reaction with the N_2O molecule. The local minima of $\text{Pt}_8\text{–N}_2\text{O}$ were determined through different approaches of N_2O on the surface of the Pt_8 particle. For the identified $\text{Pt}_8\text{–N}_2\text{O}$ low-lying states, a vibrational analysis was done, under the harmonic approximation, to confirm if they are true minima on the potential energy surface. Adsorption energies (E_{ads}) of N_2O on Pt_8 were estimated as the difference between the total energy of the complex ($\text{Pt}_8\text{–N}_2\text{O}$) and its constituents (Pt_8 and N_2O). Specifically, the following equation was used:

$$E_{\text{ads}} = E_{\text{b}}(\text{Pt}_8 + \text{N}_2\text{O}) - [E_{\text{b}}(\text{Pt}_8) + E_{\text{b}}(\text{N}_2\text{O})] \quad (1)$$

where $E_{\text{b}}(\text{Pt}_8 + \text{N}_2\text{O})$ is the binding energy of the complex $\text{Pt}_8 + \text{N}_2\text{O}$, and $E_{\text{b}}(\text{Pt}_8)$ and $E_{\text{b}}(\text{N}_2\text{O})$ are the GS binding energies of the Pt_8 and N_2O species, respectively.

For a complete reaction pathway analysis, additional geometry optimizations were performed to search for saddle points, which represent transition states (TSs). Both eigenvector-following and specification of reaction coordinates for TS search (TSRC) techniques were used. For all transition states, it was confirmed that they had only one imaginary frequency. This methodology showed to be successful to explain the reduction mechanism of N_2O on neutral, cationic, and anionic Rh_6 nanoparticles.^{33,34} For instance, it was demonstrated that, without proper inclusion of the relativistic effects by means of the ZORA formalism in the calculations for the $\text{Rh}_6 + \text{N}_2\text{O}$ reaction pathways, the neutral Rh_6 particle was not able to reduce the N_2O molecule.³⁴ Three main features are appropriately considered in the present study: (a) the exchange-correlation interactions, which are accurately described by the PBE functional; (b) the relativistic effects accounted by the ZORA approach, which approximately solves the Dirac equation; and (c) the JT effects, which were inspected for each cluster without imposing symmetry

constraints during the calculations or by explicit calculation of the low-symmetry structures of the clusters.

3. RESULTS AND DISCUSSION

3.1. Low-Lying States of the Pt₈ Cluster. Figure 1 shows the stable structures identified for the pristine Pt₈ cluster in the

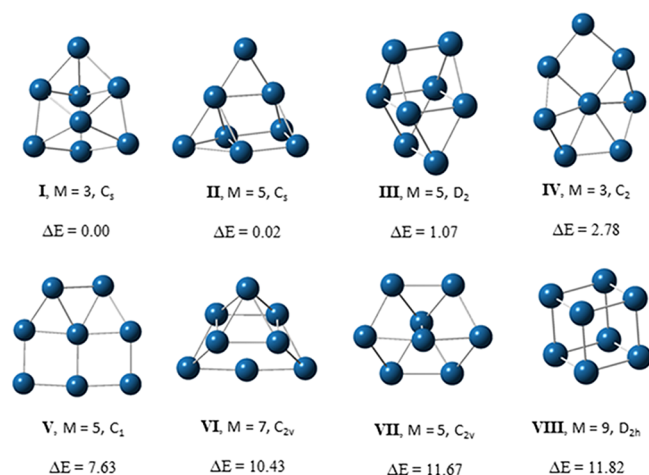


Figure 1. Determined DFT PBE-ZORA low-lying structures for the neutral Pt₈ cluster. The multiplicity, *M*, point group symmetry, and relative energy for each isomer are indicated.

present study, obtained by means of the DFT PBE-ZORA optimization calculations, which includes relativistic effects. A triple tetragonal pyramid defines the GS of Pt₈ with spin multiplicity of 3 and C_s point symmetry group. This result agrees with those found by Sebetti¹⁷ by means of the BPW91 method in concert with effective core potentials and a valence space of 18 electrons, and by Kumar and Kawazoe¹² employing a GGA approach and ultrasoft pseudopotentials; both studies indicate a triplet for the TTP ground state. The GS of Pt₈ has a cluster symmetry plane (CSP) which crosses the vertices 1, 2, 4, and 8, dividing it into two equal parts and making the 5-3 and 7-6 pairs of Pt atoms equivalent; see Figure 2. The average Pt–Pt bond length (2.61 Å) found in this work for Pt₈ is in the interval reported in the literature (2.52–2.72 Å). The shortest distance, 2.52 Å, is found for the Pt(4)–Pt(5) and Pt(4)–Pt(3) pairs, which have the Pt(4) atom lying on the CSP mirror.

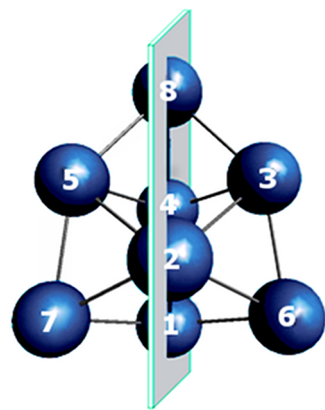


Figure 2. Triple tetragonal pyramid ground-state structure of the Pt₈ cluster. The cluster symmetry plane is indicated, as well as the labels for each platinum atom.

Larger distances, 2.60 and 2.61 Å, occur for the 7-5, 5-8, 8-3, and 3-6 pairs located at the periphery of the cluster, that is, where such atoms may be nearer to a surface behavior. Indeed, the Pt(6), Pt(7), and Pt(8) atoms are less coordinated, since they are bonded to the three nearest atoms, while the others have coordination of four and five. Also, as will be shown below, the 6, 7, and 8 sites are the ones with more negative charge. Note that the nearest neighbor distance of the *fcc* Pt bulk is 2.78 Å.³⁵ Thus, shorter bond lengths occur on the Pt₈ cluster, due to its lower coordination numbers (3, 4, and 5) as referred to that of the bulk (6), forming stronger Pt–Pt bonds and a magnetic moment of 2 bohr magneton (μ_B). The isomer with a null magnetic moment, *M* = 1, appears near in energy (3.25 kcal/mol) to the GS, while the septet is also close; see Table 1. As will be discussed below, aside from the TTP isomers, we found that other structures, presenting different spin states, also are near in energy to the GS; see Figure 1. These isomers, of different geometry and multiplicity, may appear in the synthesis of Pt₈ in the gas phase, yielding magnetic behavior with a magnetic moment roughly equal to the average value of such states. Though not exactly the same size as the cluster, our estimated average magnetic moment for the Pt₈ cluster, 0.46 μ_B per atom for the located isomers quoted in Table 1, is consistent with the measured values (0.27–0.38 μ_B /atom from XANES and XMCD spectra and 0.65 μ_B /atom using the SQUID magnetometer data) for the Pt₁₃ particle supported on a zeolite.^{3,4}

The PBE-ZORA method reveals that several states are near in energy to the TTP GS; see Table 1. For instance, isomer II, a bi-capped triangular prism with two ad-atoms located on a triangular face and bridging an edge between square faces, with point group C_s and multiplicity 5, differs negligibly in energy, 0.02 kcal/mol, from the GS. This isomer corresponds to the second low-lying state reported by Sebetti.¹⁷ It fits also with the fifth one found by Li et al.²¹ Isomer III is a bi-prism with perpendicular top and bottom edges and closely resembles both the GS determined by means of the UPBE0/def2-TZVP method²⁰ and the GS determined by means of the meta-GGA (TPSSH) functional with cc-pVTZpp basis sets.²¹ The spin states of isomer III have multiplicities of 5, 7, and 3, and they appear also very near in total energy—1.07, 1.31, and 1.72 kcal/mol, respectively—to the TTP fundamental state. They have the next point group symmetries: D₂ (*M* = 5), D_{2d} (*M* = 7), and D₂ (*M* = 3); see Table 1. We found that the D₂ low symmetry of the quintet and triplet states of isomer III originate from JT distortions of the D_{2d} isomer. That is, the quintet bi-prism isomer III, of lower symmetry, D₂, shows the importance of JT effects in the low-lying states of Pt₈. In fact, most isomers we determined for this cluster break their original symmetry.

Isomers IV and V are quasi-planar structures; the former corresponds with the GS found by Chaves et al.,¹⁹ whereas the latter resembles the second isomer obtained by Kumar and Kawazoe.¹² In this work we found that isomer IV with *M* = 3 is also near, less than 3 kcal/mol, to the TTP GS, implying a competition between 2D and 3D isomers to lie close to the GS, whereas the quintet of isomer IV is located at higher energy, 6.10 kcal/mol. We also found that the quasi-planar isomer V, with a multiplicity of 5, lying at 7.63 kcal/mol, is also a higher energy state. That is, quasi-planar, planar, and three-dimensional structures of Pt₈, in different spin states, are contained within less than 8 kcal/mol. This diversity of isomers near to the GS complicates the decision of which to choose in the first instance to study as catalyst for the N₂O reduction. In this case,

Table 1. Isomeric Structures for the Pt₈ Cluster: Symmetry, Magnetic Moment, Relative Energies, in kcal/mol, Bond Lengths, HOMO–LUMO Gaps, and Vibrational Frequencies for Each Isomer

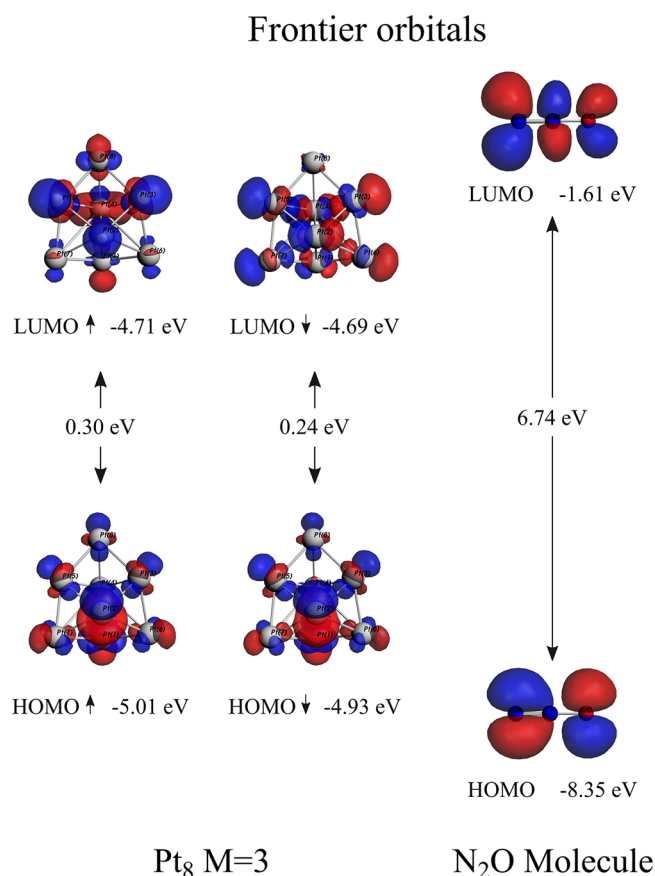
isomer	symmetry group	magnetic moment (μ_B)	relative energy (kcal/mol)	bond length range (Å)	α HOMO–LUMO gap (eV)	β HOMO–LUMO gap (eV)	vibrational frequencies range (cm ⁻¹)
I	C _s	2	0.00	2.52–2.61	0.30	0.24	45–207
II	C _s	4	0.02	2.46–2.68	0.15	0.35	21–235
III	D ₂	4	1.07	2.52–2.60	0.09	0.40	44–199
III	D _{2d}	6	1.31	2.53–2.59	0.44	0.11	46–202
III	D ₂	2	1.72	2.52–2.59	0.49	0.34	44–194
IV	C ₂	2	2.78	2.45–2.58	0.43	0.15	31–227
I	C _s	0	3.25	2.51–2.61	0.06	–	53–204
I	C ₁	6	5.06	2.55–2.61	0.19	0.19	37–199
IV	C ₁	4	6.10	2.47–2.62	0.41	0.16	30–228
V	C ₁	4	7.63	2.43–2.63	0.76	0.13	13–228
VI	C _{2v}	6	10.43	2.54–2.67	0.22	0.12	34–205
III	D _{2d}	0	11.59	2.49–2.56	0.03	–	64–212
VII	C _{2v}	4	11.67	2.54–2.62	0.46	0.13	35–197
VIII	D _{2h}	8	11.82	2.51–2.56	1.32	0.01	28–180

we selected isomer I because, in the literature, a cluster of such low symmetry has not been studied as a potential N₂O catalyst. This makes it particularly interesting because multiple reaction pathways that compete with each other exist.

Lastly, a pair of structures lying farther away from the GS were located: isomer VII, which is a distorted hexagonal bipyramid with $M = 5$ and C_{2v} symmetry, and the cubic JT distorted D_{2h} structure, isomer VIII, with a larger multiplicity, $M = 9$. They appear at higher energies, 11.67 and 11.82 kcal/mol, respectively. Note that the prototypical (bulk) cubic structure, in a nonet spin state, appears with slight deviations from the O_h symmetry, due to the JT effect. This is important since the cubic form was determined as the lowest energy state for Pt₈ in previous studies. For instance, Xiao and Wang,⁸ using a GGA scheme and a pseudopotential with a 5d¹⁰6s¹ valence space, found a compact cubic O_h structure of high spin, 8 μ_B , and sides of 2.54 Å. Hamad et al.,¹⁸ employing the PBE functional and an ultrasoft pseudopotential, determined a cubic form of 2.54 Å and with 8.14 μ_B . We found also at high energy another 3-4-1 structure of high multiplicity, $M = 7$; this is isomer VI in Figure 1. Overall, “bulk” structures appear at higher energy with large magnetic moments, whereas more compact and planar motifs, not resembling fragments of the bulk, with low magnetic moments, define the low-lying states of the Pt₈ cluster. Despite the lack of experimental information about Pt_n in the gas phase, several clusters have been synthesized and deposited on diverse surfaces.^{36–38} Watanabe et al.³⁶ reported the transition from 2D to 3D structures with Pt_n ($n \geq 8$) clusters deposited on TiO₂ (110) surfaces, although other authors claim that the transition takes place from larger clusters.^{37,38}



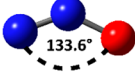
Small HOMO–LUMO gaps, ≤ 0.30 eV, occur for the TTP GS of Pt₈, suggesting high reactivity for this particle. Figure 3 contains the HOMO and LUMO contour plots for the separate Pt₈ and N₂O systems. In the LUMO of Pt₈, the atoms show clearly 5d signatures, and some sites present partial positive charges. For instance, the Pt(1) atom presents a positive charge of +0.012 electron (e). As will be shown below, in one of the low-lying states of the Pt₈–N₂O complex, the N₂O molecule is *atop* absorbed on the Pt(1) site. Another low-lying state is the *bridge* absorption of N₂O on the Pt(7)–Pt(1) side.

Furthermore, one electron detachment from the TTP $M = 3$ GS produces a quartet for the Pt₈⁺ ion. The difference in total

**Figure 3.** Frontier orbitals, HOMO and LUMO, for the ground states of the Pt₈ and N₂O systems. The energy gaps are also indicated.

energies between the charged, Pt₈⁺, and neutral, Pt₈, optimized species gives an adiabatic ionization energy (IE) of 6.90 eV (7.04 eV). Similarly, the lowest energy state of the Pt₈[−] anion is a doublet, and the electron affinity (EA) is 2.95 eV (2.82 eV). [The vertical IE and EA are in parentheses.] These IE and EA results, either adiabatic or vertical, indicate a chemical potential, μ , of −4.93 eV for the Pt₈ cluster in the gas phase. This finding matches the value reported by Heredia et al.,¹⁶ albeit for the cubic lowest energy structure of this cluster. Photoelectron spectra have been previously reported for charged clusters Pt_n[−]

Table 2. Multiplicities (*M*), Total Charge (*Q*), Bond Lengths, Vibrational Frequencies, ν , Geometries, and Atomic Charges (*q*) for Neutral and Charged Species of the N₂O Molecule

<i>M</i>	<i>Q</i>	Structural Parameters		Frequencies ^a (cm ⁻¹)			Geometry ^b	Hirshfeld charges		
		<i>d</i> _{N-N} (Å)	<i>d</i> _{N-O} (Å)	ν_1	ν_2	ν_3		<i>q</i> _{N End}	<i>q</i> _{N Central}	<i>q</i> _O
1	0	1.137	1.19	2275.9 (2224.2)	1297.0 (1285.3)	595.6 (588.2)		-0.08	0.19	-0.11
2	+1	1.159	1.18	2291.5	1278.8	701.9		0.32	0.38	0.30
2	-1	1.206	1.33	1602.9	963.4	652.0		-0.42	-0.11	-0.47

^aExperimental values are given in parentheses.⁴² ^bThe adiabatic electron affinity of the N₂O molecule is -0.47 eV, and its ionization energy is 12.98 eV.

($n \leq 7$) in the gas phase³⁹ as well as for deposited small platinum clusters,^{39–41} but the corresponding spectrum for Pt₈ has not been reported.

For N₂O, the estimated distances, $d(\text{NN}) = 1.137$ Å and $d(\text{NO}) = 1.192$ Å, signify stability for this molecule, as they are short, which is consistent with its large HOMO–LUMO gap of 6.74 eV; see Figure 3. These computed parameters are near to the experimental values: $d(\text{NN}) = 1.128$ Å and $d(\text{NO}) = 1.184$ Å.⁴² Furthermore, they indicate that the length of the N–N–O molecule, 2.312 Å (experiment) or 2.329 Å (theory), is a bit shorter than the typical Pt–Pt distances, 2.517–2.612 Å, of the Pt₈ particle, which makes favorable first the adsorption and then the activation of the N₂O molecule on some Pt–Pt sides of the catalyst. The experimental results of IE (12.89 eV) and EA (−0.15–0.76 eV) allow the estimation, −6.37 to −6.83 eV, of the chemical potential of the N₂O molecule. The PBE-ZORA method yields an adiabatic IE of 12.98 eV, close to the experimental value, and an EA of −0.47 eV, yielding a chemical potential of −6.23 eV. That is, since the chemical potential of the N₂O is smaller than that of the Pt₈ cluster, transference of electrons may occur from the metal catalyst toward the N₂O reactant. The transferred charge goes into the antibonding LUMO of N₂O, weakening the N–O bonding. Note also that the population analysis indicates that both terminal nitrogen and oxygen sites have partial negative charges, with the latter having the biggest value. These features are important for the mechanism of the N₂O + Pt₈ reduction reaction, since in the earlier reaction steps the O atom and the N-terminal site need to interact with the Pt atoms on the cluster surface through a charge-transfer process. The Pt₈ cluster presents the ideal conditions to form an adduct with N₂O adsorbed in *bridge* as a precursor to dissociation of the molecule.

The calculated lowest energy structure of the N₂O anion, shown in Table 2, indicates that the Pt₈-to-N₂O transference of charge, quoted above, may weaken the bonding of the N₂O molecule. One-electron addition produces strong structural changes on the neutral N₂O molecule. Effectively, the anion presents a bent structure instead of a linear one, with an N–N–O angle of 133° and with a clear lengthening of the N–N (1.206 Å) and N–O (1.325 Å) distances, as referred to those of the neutral N₂O (1.137 and 1.192 Å). To the contrary, the N₂O⁺ ion remains linear, with shorter N–O bond length and slightly larger N–N distance.

3.2. Coordination Modes of N₂O on the Pt₈ Particle. Our search for the reaction pathways starts by studying the

adsorption of the N₂O molecule on the different non-equivalent sites for the GS structure of Pt₈, as a necessary stage in the reduction process. We studied all three possible adsorption configurations: (i) *atop*, (ii) *bridge*, and (iii) *hollow* (face-centered). The relevant geometrical parameters for each adsorption configuration are summarized in Table 3; only the

Table 3. N₂O Binding Energy (*E_b*), Pt–O Distance (*d*_{Pt–O}), Shortest Pt–N Distance (*d*_{Pt–N}), Average Pt–Pt Distance (*d*_{Pt–Pt}), and N–N Stretching Frequency ($\nu_{\text{N–N}}$) Computed for N₂O Adsorbed on Pt₈ with Different Adsorption Configuration and Non-equivalent Sites

adsorption configuration	sites	<i>E_b</i> (kcal/mol)	<i>d</i> _{Pt–O} (Å)	<i>d</i> _{Pt–N} (Å)	<i>d</i> _{Pt–Pt} (Å)	$\nu_{\text{N–N}}$ (cm ⁻¹)
<i>atop</i>	5	−19.09		1.96	2.59	1254
	7	−19.15		1.93	2.59	1254
	2	−17.87		1.97	2.59	1258
	1	−22.94		1.95	2.58	1255
	4	−19.24		1.97	2.59	1258
	8	−14.74		1.98	2.62	1244
<i>bridge</i>	5-7	−19.50	1.99	1.96	2.6	1526
	5-8	−19.50	1.99	1.96	2.64	1526
	5-2	−14.10	2.04	1.96	2.59	1556
	7-5	−21.27	2.05	1.95	2.59	1508
	7-2	−18.05	2.06	1.95	2.62	1520
	7-1	−21.95	2.03	1.91	2.60	1528
	2-5	−19.50	1.98	1.9	2.61	1515
	2-7	−14.11	1.99	1.94	2.57	1525
	4-5	−11.48	2.10	1.98	2.59	1580

lowest energy configurations are presented there. Their graphical representations are shown in the Supporting Information, Figure S1 for the *atop* modes and Figures S2–S4 for the *bridge* (central graph) ones. The adsorption *atop* N-bound always exceeded the O-bound, since the latter resulted in energies lower than 3 kcal/mol, and *hollow* did not prove to be a favorable adsorption mode; thus, it does not appear in Table 3. All the N-bound *atop* configurations fall in the chemisorption regime. This characteristic has been observed in other metal clusters adsorbing nitrogen-containing molecules. Even though several nitrogen-containing metallic clusters show the nitrogen bonded to the cluster in a *bridge* position,^{43,44} the most commonly found configuration is the N-bound *atop*.^{45–52} In particular, rhodium clusters^{49,50,53,54} and surfaces^{55,56} have

proved to serve as catalyst in the N_2O reduction through its adsorption on *atop* sites. In fact, the binding energy (E_b) of the N_2O unit is -22.94 kcal/mol for site 1, producing the lowest energy $\text{Pt}_8\text{-N}_2\text{O}$ structure. A smaller E_b , -14.74 kcal/mol, is found for site 8. This notable difference for E_b reveals a sensitivity of the cluster site involved in the absorption process. Note that the Pt(1) and Pt(8) atoms are on opposite sites on the CSP of Pt_8 : tip and bottom points, respectively. It is possible to appreciate in Figure 3 that the HOMO of the Pt_8 cluster has significant signatures on the Pt(1) site, which has positive charge ($+0.01e$). Thus, site 1 is favorable for a bonding interaction with the terminal N atom of N_2O , which has negative charge and signatures on the HOMO level; see Table 2. In contrast, it will be less favorable for the Pt(8) site, having a negative charge ($-0.05e$) and smaller contributions on the HOMO level, to form a bond with the N_2O molecule. These electronic features roughly account for the larger difference between $E_b(1)$ and $E_b(8)$. The 1 and 8 *atop* absorption modes of N_2O are shown in Figure 4. Note also that site 1 is the strongest electrophilic site, while site 8 is a weak nucleophilic site.

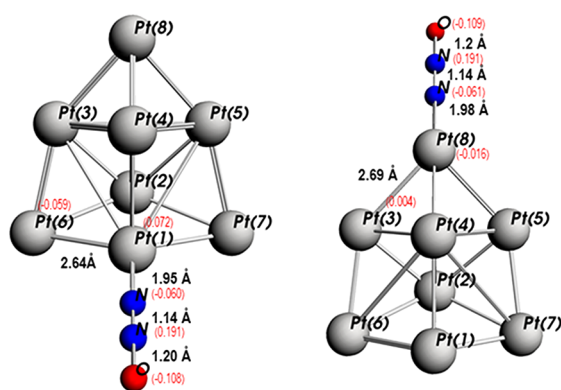


Figure 4. Lowest energy structures for the $\text{Pt}_7\text{Pt}(1)\text{-N}_2\text{O}$ and $\text{Pt}_7\text{Pt}(8)\text{-N}_2\text{O}$ *atop* coordination modes. The Hirshfeld charges on the N_2O moiety and on the nearest Pt atoms are indicated.

Consistent with the chemisorption energies, short Pt–N bond lengths appear for the *atop* coordination, e.g., 1.95 Å for the $\text{Pt}_7\text{Pt}(1)\text{-N}_2\text{O}$ absorption. The largest value, 1.98 Å, occurs for the $\text{Pt}_7\text{Pt}(8)\text{-N}_2\text{O}$ mode. The shortest metal–ligand bond length (1.93 Å) occurs for the $\text{Pt}_7\text{Pt}(7)\text{-N}_2\text{O}$ mode. In the *atop* absorption modes, the structure of the Pt_8 cluster is roughly preserved, which is important for what follows. Even more, in the *atop* absorptions, the linear geometry of the N_2O molecule is nearly preserved, and a small lengthening of the N–O bond, by about 0.01 Å, is produced, whereas that of the N–N bond is negligible. This indicates the absence of a charge-transfer process from the metal toward the N_2O molecule. As a matter of fact, the *atop* adsorbed N_2O molecule presents small positive charges instead of negative; see Figure 4.

Most of the binding energies for the *bridge* modes are near to the *atop* ones, showing that the Pt–O bonding, unlike Pt–N, does not significantly contribute to the stability of the $\text{Pt}_8\text{-N}_2\text{O}$ complex. This may be due to the increase of the metal–ligand repulsion in the *bridge* modes, where the atoms of the (rich in electrons) N_2O molecule are nearer to those of the (also rich in electrons) metal atoms of the cluster. On the other hand, for the *atop* modes the electronic density of the ligand points away from the metal.

The similarity in E_b values for the *atop* and *bridge* coordination modes is illustrated by the *atop* binding energy on site 5 of -19.09 kcal/mol, as compared to the value of -19.50 kcal/mol for the 5-7 and 5-8 *bridge* modes. In contrast, the *bridge* sites 5-2 and 4-5 are 4.99 and 7.76 kcal/mol smaller, respectively, than those for the *atop* sites 5 and 4 N-bound platinum sites. Furthermore, asymmetries on the *bridge* adsorption, with respect to the atomic exchange, are evident from the E_b values quoted in Table 3. Indeed, comparing the E_b 's of the pairs (5-2, 2-5) and (7-2, 2-7), differences of about 5 kcal/mol emerge, marking the sensitivity of the cluster site where the O-bound and N-bound are formed. This is more evident for the 5-8, 7-1, and 4-5 pairs, which do not have their respective counterparts because the N_2O molecule resulted in desorption for these cases. In general, a *bridge* formation was not favorable for two Pt atoms lying on the CSP, where the electronic density of the cluster is high. These asymmetries, revealed by the differences in binding energies and the absence of adsorption, depend on the orientation of the molecule, NNO or ONN, and on the specific adsorption sites of the cluster surface. That is, they are a natural consequence of the low symmetry of the Pt_8 cluster and the intrinsic structural inhomogeneity of the N_2O molecule. Nevertheless, it is interesting that the cluster presents so many possibilities to start the reduction reaction of N_2O , and to carry out this process with low barrier energies. This fact is attributed to the hybridization possibilities of the platinum s and d orbitals, making localized and delocalized Pt–Pt bonds, depending on the nature of the s-d hybridization.

The preference of N_2O for binding by the N terminal site is seen from the shorter $d_{\text{Pt-N}}$ distances as compared with the $d_{\text{Pt-O}}$ ones in the *bridge* modes presented in Table 3. Note that the Pt–N bond lengths have no substantial difference between the *bridge* and *atop* low-lying states. A clear difference between *atop* and *bridge* configurations is revealed by the significant blue shift (~ 270 cm^{-1}) of the $\nu_{\text{N-N}}$ stretching frequency in the transition from *atop* to *bridge*. This feature, indicating a reinforcement of the N–N bonding and being in agreement with a Pt–O bond formation, allows us to predict possible oxygen activation. As we will show later, this activation is crucial to produce spontaneous dissociation of N_2O on the Pt_8 surface.

The structural preservation of the Pt_8 cluster is apparent from the average $d_{\text{Pt-Pt}}$ distance calculated for the different adsorption cases. However, this fact can be misleading; in fact, the cluster can suffer considerable distortion on the *bridge* modes, being mainly produced by changing the positions of the atoms bonded to the N–N–O molecule. These atomic rearrangements can be asymmetric, rooted in the asymmetry of the adsorbed molecule. For example, Figure 5 shows the *bridge* adsorption structures and HOMOs for 2-7 (a) and 7-2 (b). In the 2-7 case, a shortening of the 2-7 bond to 2.57 Å and an enlargement to 2.67 Å of the reflected bond (by the CSP) 2-6 are produced by the adsorption. In contrast, in 7-2 a much bigger enlargement of the bond 2-7 to 3.27 Å occurs, accompanied also by a small lengthening, to 2.64 Å, of the reflected bond 2-6. It is important to remark that the 2-6 and 2-7 bonds are symmetric, with the same length (2.60 Å) in the pristine Pt_8 cluster. This type of structural relaxation signifies great fluxionality of the Pt_8 particle that allows it to rearrange, making possible opposite *bridge* adsorptions of N_2O , with a binding energy difference of around 4 kcal/mol. The HOMO for the 2-7 *bridge* shows $d\pi\text{-}p\pi$ bonding between N_2 and Pt(2), having as a consequence the weakening of the N–O bond,

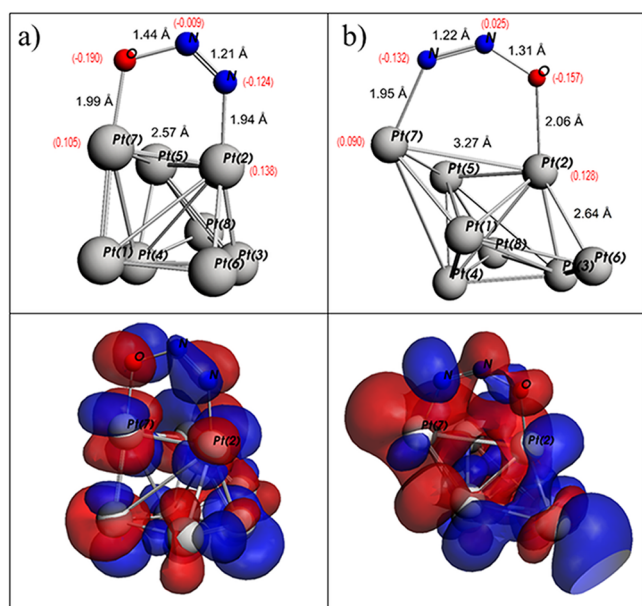


Figure 5. Structures for the (a) 2-7 and (b) 7-2 bridge N_2O - Pt_8 adsorptions modes. Contour plots for the corresponding HOMO level are depicted below the structures.

which is in line with a considerable lengthening, from 1.137 to 1.440 Å, for this N–O bond. Note also the transference of charge, $-0.323e$, into the antibonding MOs of N_2O , which ultimately accounts for the weakening of the N–O bond. Instead, a smaller charge transfer, $-0.264e$, occurs in the 7-2 bridge, producing smaller enlargement for the N–O bond distance; see Figure 5. Note that the HOMO for the 7-2 bridge shows σ bonding between Pt(7) and the central N atom, which accounts for the increase of the binding energy for the 7-2 bridge. Thus, large fluxionality occurs in this 7-2 interaction, which will have produced one of the more favorable reaction pathways for the N_2O reduction.

3.3. Reaction Pathways for the Reduction of the N_2O Molecule. We now focus our discussion on the reduction process of N_2O on the surface of the Pt_8 cluster. All the possible reaction pathways were explored, considering the multiple non-equivalent sites presented by Pt_8 . A large number of reduction routes, 11, were found for the low-symmetry Pt_8 cluster, acting as catalyst. Such multiple reactions have regio selective character, which does not occur in more symmetric clusters. However, for illustrative purposes, we will discuss only three representative reaction pathways: 5-7, 7-2, and 8-5, depicted in Figures 6 and 7. The first presents the lowest barrier and the second the highest one, whereas 8-5 is one of the reaction pathways yielding spontaneous dissociation without forming the bridge. Furthermore, several routes, for instance 5-4 and 8-4, were unfavorable for reduction, leading to desorption. In Figures 6 and 7, the Pt_8 - N_2O configurations for each stage are included (the complete reaction adducts are included in Figures S2–S5).

The reaction starts (stage 2 in Figures 6 and 7) by means of N-bonds, N_2O seats on the Pt_8 cluster yielding *atop* modes, where the stabilization energies depend markedly on the adsorption site; see Table 3. As mentioned, in this stage the reactive N_2O keeps its linear shape, with the N–N lengthening indicating the beginning of the activation process. Overall, there are two transition states in the whole reduction process of N_2O on the cluster surface: TS1^\ddagger between *atop* and *bridge* local

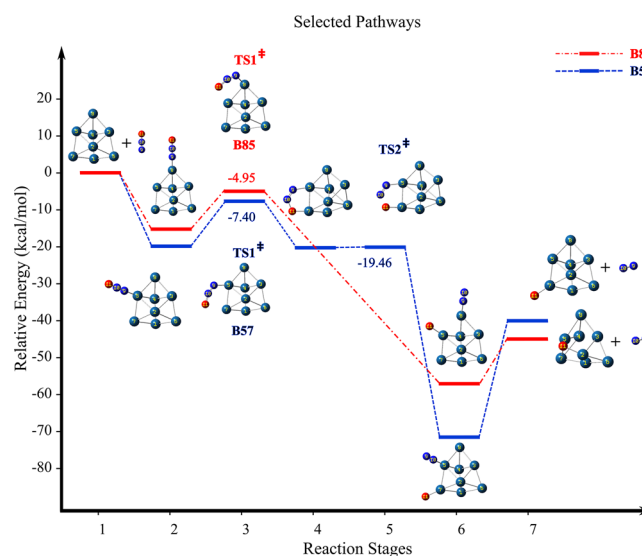


Figure 6. Energy profile diagram for the bridge B57 and B85 reduction reactions of N_2O on the Pt_8 cluster. Reactants, local minima intermediates, transition structures, and products are indicated.

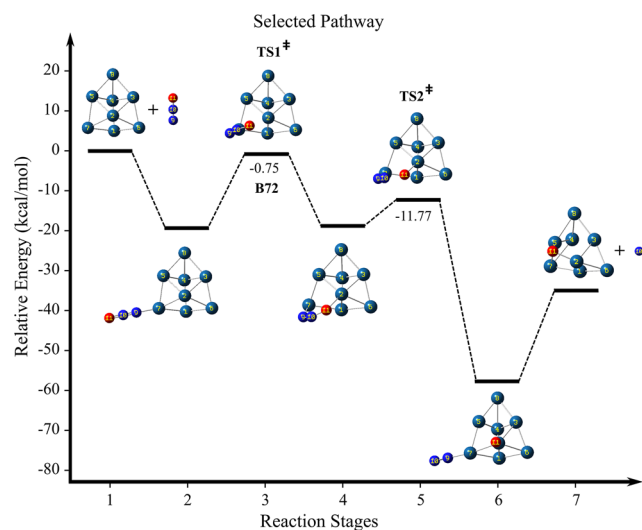


Figure 7. Energy profile diagram for the B72 reduction reaction of N_2O on the Pt_8 cluster. Reactants, local minima intermediates, transition structures, and products are indicated.

minima, and TS2^\ddagger between *bridge* and the dissociated ($\text{N}_2 + \text{O}$) products on the Pt_8 surface. Binding energies, barrier heights, and relevant geometrical parameters of the N_2O molecule for each transition state (TS1^\ddagger and TS2^\ddagger) are summarized in Table 4.

Now we are going to describe these reaction pathways. From the *atop* adsorption modes to stage 3, the N_2O molecule is rotated toward one nearby platinum atom, giving the activated complex TS1^\ddagger , whose binding energy depends significantly on the orientation reached, as can be appreciated in Table 4. Note that TS1^\ddagger is a frustrated bridge configuration, because the Pt–O bond formation is not fully achieved. As we mentioned before, bridge formation was not favorable for two Pt atoms on the CSP mirror because no transition structures appear in those directions. The reaction barriers reported in Table 4 show that the pathways toward the bridge formation at the lateral Pt–Pt bonds (8-5, 5-7, 5-8, 7-5) are more favorable than those

Table 4. N₂O Binding Energy (E_b), Barrier Height, N–O Distance (d_{N-O}), and N₂+O Binding Energy (E_{dis}) Computed for the N₂O Adsorbed Molecule on Pt₈, for Different Non-equivalent Bridges

bridged atoms	TS1 [‡]			TS2 [‡]			
	E_b (kcal/mol)	barrier height (kcal/mol)	d_{N-O} (Å)	E_b (kcal/mol)	barrier height (kcal/mol)	d_{N-O} (Å)	E_{dis} (kcal/mol)
5-7	−7.4	11.69	1.22	−19.46	0.04	1.48	−69.11
5-8	−6.83	12.26	1.23	−19.46	0.04	1.48	−62.8
5-2	−1.92	17.17	1.22	−13.65	0.45	1.50	−58.36
7-5	−7.43	11.72	1.22	−20.30	0.97	1.53	−53.28
7-2	−0.75	18.4	1.23	−11.77	6.28	1.63	−64.69
7-1	−1.77	17.38	1.22	−19.86	2.09	1.54	−57.03
2-5	−4.15	13.72	1.23	−19.37	0.13	1.51	−64.69
2-7	−2.55	15.32	1.24	−14.09	0.02	1.50	−55.41
1-7	−7.94	15.00	1.23				−66.59
4-5	−6.58	12.66	1.23	−9.19	2.29	1.57	−70.63
8-5	−4.95	9.79	1.22				−58.47

including atoms on the CSP mirror. For instance, for 5-4 the reaction barrier is larger than the desorption energy, preferring this last channel, and it is not included in Table 4. Likewise, the desorption channel is strongly favored for the reaction pathways passing through 5-2, 7-2, 7-1, and 2-7 frustrated bridges, all involving atoms on the CSP mirror, but that is not so for the reflected frustrated bridges 1-7 and 2-5. Roughly speaking, around 42% of the reaction pathways end in desorption. Besides that, note the large asymmetry between some of the reaction barriers, such as the ones found for 8-5 and 5-8. This is in concordance with the asymmetries related with the NNO (ONN) bridge bond formation, discussed above. For the cases of Figures 6 and 7, the transition structures TS1[‡] are characterized by Pt(a)–Pt(b)–N angles of 85.6°, 89.5°, and 88.4°, Pt(b)–N–N angles of 130.4°, 123.7°, and 126.4°, and N–N–O angles of 152.1°, 149.4°, and 152.3° for 5-7, 7-2, and 8-5, respectively, where a–b are the bridged platinum sites. This means two things: (1) in the TS1[‡] stage there is a tendency to form a *bridge*, which is evidenced from the diminution of the Pt(a)–Pt(b)–N angles whose values in the previous *atop* stage are 103.5°, 133.2°, and 119.2° for 5-7, 7-2, and 8-5, respectively, and (2) an important N–N–O bending is promoted, since the *atop* modes showed a quasi-linear configuration for this molecule when it was adsorbed. Note also the slight elongation of the N–N and N–O bond lengths (Figures S2–S5), confirming the switch-on of activation for the N₂O molecule in this transition-state step.

Afterward, in a bent geometry, the NNO molecule bridges in a parallel way to a Pt–Pt bond (stage 4). As we mentioned previously, most of the bonding energies of *bridges* are degenerated with *atop* modes. However, the *atop* channel is preferred to start the reaction, because it does not require any rearrangement of N₂O on the Pt₈ surface. The reaction barriers TS1[‡] are the necessary energies to do these configurational changes, which have values of 9.79–18.4 kcal/mol. Leaving aside the cases where the N₂O desorption channel is more favorable, the activation energy is about 15.0 kcal/mol for the 1-7 route. These barrier heights are competitive with that obtained for cationic Rh₆ ionized clusters³³ and achievable for infrared pumping of the adsorbed N₂O vibrational modes.⁵⁷ At room temperature, no Pt₈ + N₂O adducts have been found from experiments of N₂O reduction in the gas phase by isolated neutral platinum clusters, using mass spectroscopy.²² The reaction products obtained for this reaction are invariably Pt₈O + N₂. Gibbs free energy profile calculations, for our reaction pathways, indicate that they occur spontaneously at room

temperature, in concordance with the experiment. The *bridge* stage is very close energetically to the transition structure TS2[‡], with a reaction barrier lower than 2.3 kcal/mol for all the studied *bridges*. Similarly, *bridge* and the TS2[‡] stages for the selected 5-7 and 7-2 modes, shown in Figures 6 and 7, are characterized by Pt(a)–Pt(b)–N angles of 83.1° (83.1°) and 78.4° (76.4°); Pt(b)–N–N angles of 129.5° (130.5°) and 128.2° (135.5°); and N–N–O angles of 121.8° (120.2°) and 132.4° (122.2°) for 5-7 and 7-2, respectively. [Values in parentheses are for the TS2[‡] stage.] These results show important rearrangements of N₂O on the surface of the cluster. This is clearly seen in Figure S6, showing also the largest change in the N–O distance, from 1.31 to 1.63 Å for such steps, which is produced by a large charge transference from Pt₈ to N₂O.

In fact, the stage 5 TS2[‡] is characterized by a large elongation of the N–O bond by around 0.3 Å in average; see Table 4. Once the reaction arrives at TS2[‡], the N₂O dissociation proceeds. For most cases, with the reaction barrier being so low, the N₂O reduction is already activated from the *bridge* molecular complex. An exception presented in Figure 7 is the reaction 7-2; in this route a double barrier toward the reduction is encountered, with the second barrier about one-third of the first one. Moreover, two reaction pathways were found in our work that activate the reaction without going through stages 4 and 5: the 8-5 (see Figure 6) and the 1-7. The first is the most probable reduction pathway, also showing the smaller barrier. Notice that the tip Pt(8) atom is where the 8-5 path started and that it had the lowest adsorption energy on the *atop* mode.

In stage 6, the N₂O molecule experiences dissociation, with the N₂ and O fragments adsorbed on the platinum atoms where the bridge was established. It is important to note the large anisotropy in the binding energies (E_{dis}) of the complex with the dissociated products (N₂ + O) bonded on the cluster surface (see Table 4), which results from additional rearrangement of the Pt atoms within the cluster to reach stable configurations. Finally, in the last stage, the Pt₈O + N₂ reaction products are formed. Depending on the final position of the oxygen atom, either *atop* or *bridge* bonding may be more favorable. In Table S1, the reaction energies released after the N₂ desorption step, for the two oxygen adsorption configurations, *atop* and *bridge*, are compiled. The *bridge* adsorption mode in small platinum cluster oxides has been experimentally confirmed by means of IR-MPD studies.^{49,58} Also, similar IR-MPD studies regarding the dissociation of N₂O on rhodium clusters, supported by DFT calculations, gave dissociation

pathways almost identical to those in the present work (pathways 8-5 and 5-7).^{49,50,54} According to these references, the N₂O first *atop* bonded, reaching a frustrated *bridge* transition state, followed by a *bridge* mode and a pre-dissociated mode, yielding dissociated N₂ and O, both *atop* bonded. Moreover, the energy barriers calculated for those systems are comparable to the one obtained in this work for the Pt₈ particle, ranging from 11.5 to 23 kcal/mol. The reaction Pt₈ + N₂O → Pt₈O + N₂ is exothermic, the released energies falling in the 28.27–44.28 kcal/mol range.

3.4. Charge-Transfer Analysis. Figure 8 has the chromatic diagrams of the Hirshfeld charges for the different reaction stages corresponding to the 5-7, 7-2, and 8-5 paths discussed above (the numerical values are in Tables S1–S3). The labels for the platinum atoms follow the representation of Figure 2, respected throughout this work, whereas the N–N–O molecule has the numeration 9-10-11. A chromatic diagram of the Hirshfeld population allows us to visualize in detail how the charges are transferred on each reaction stage. The charge transfer for each step is as follows. In the first stage, the reactants present an inherent polarization, with the Pt(1) up to the Pt(5) atoms presenting small positive charges, while the atoms lying on the Pt(6), Pt(7), and Pt(8) vertexes have negative charges. Pt(4) has the maximum positive charge (0.078e), whereas Pt(8) appears with the largest negative charge (−0.055e); both sites belong to the CSP plane (see Figure 2). The N₂O molecule has the known charge pattern N^{δ−}N^{δ+}O^{δ−} for this stage of separated Pt₈ and N₂O species. However, with bigger or smaller atomic charges, such a pattern will remain for all Pt₈ + N₂O reaction stages before the N₂O dissociation.

We can see in Figure 8 how the charge evolves as the reaction progresses. For the pathway B57 (Figure 8a) the pair of atoms, 5 and 7, that will participate in the *bridge* bond formation open a natural channel to transfer negative charge from Pt₈ toward N₂O, which is carried out until after the third stage, because in the *atop* local minima the net charge on the absorbed N₂O molecule is clearly positive (0.032e). This expected contribution appears in Figure 8a as the tendency of the columns for Pt(5) and Pt(7) toward the light blue color as the stages progress. There is also a partial negative charge transfer to the molecule from the tip Pt(8) site which is discharged in the two stages before dissociation, *bridge* and TS2[‡]. That is, it has smaller negative charges in those stages than in the pristine Pt₈ cluster; see Figure 8a and Table S2. Although with a smaller transference of negative charge, the Pt(6) site presents a similar behavior as Pt(8). In stage 5, for TS2[‡] the net charge transferred to N₂O presents the largest value, $q = -0.305e$, accounting for the considerable weakening of the N₂O molecule at this stage. Lastly, we can observe also in Figure 8a that the terminal N(9) and O(11) atoms receive all the negative charge during all the reaction stages. This is consistent with the fact that those atoms are the ones that are directly bonded to the Pt(5) and Pt(7) atoms. Note that the negative charge is mainly concentrated in the O atom in the dissociation stage 6, making a rich or high electron density on that Pt–O region. Thus, the Pt₈O oxide system may be more reactive than the pristine bare cluster.

For the pathway 7-2, Figure 8b, the charge-transfer mechanism is like the 5-7 one, but involving atoms Pt(7) and Pt(2). The tendency toward light blue color is highlighted in columns Pt2 and Pt7, not involving another atom notably. For stage 2, a net positive charge transfer (0.032e) to N₂O is also

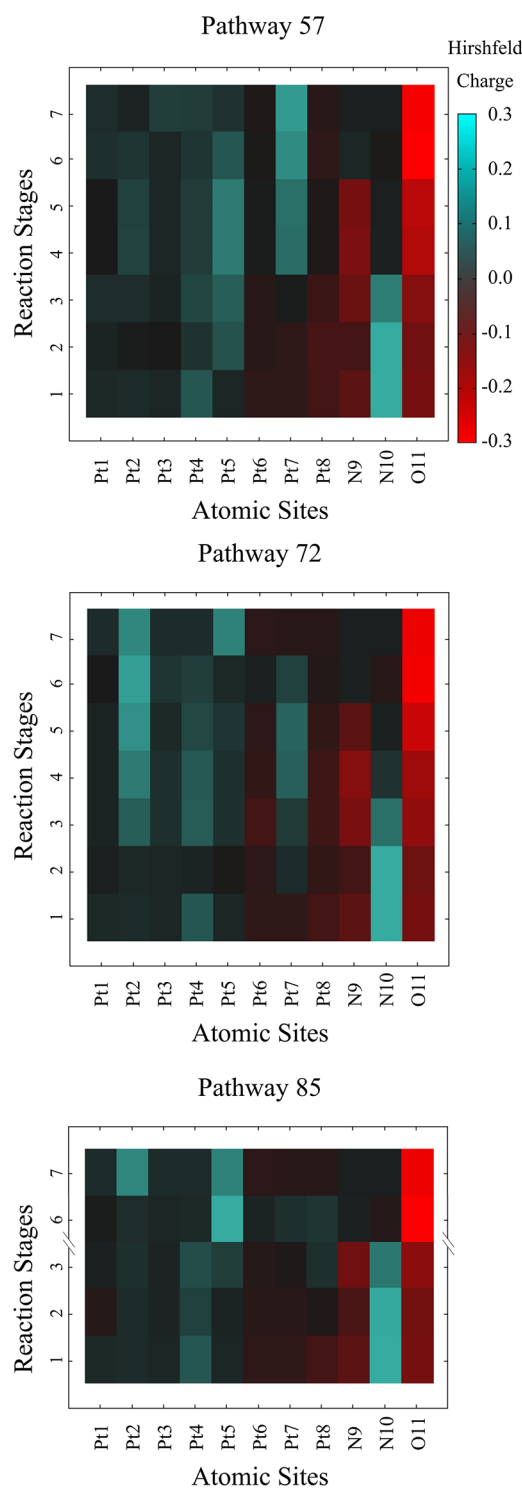


Figure 8. Chromatic diagrams of the Hirshfeld charges on the Pt(1–8) atoms, and the N (9, 10) and O (11) atoms for each reaction stage corresponding to the (a) B57, (b) B72, and (c) B85 reaction pathways.

found (see Table S3), which begins to reverse until reaching $q = -0.288e$ in stage 5 before dissociation. Again, the terminal N(9) and O(11) atoms concentrate all the negative charge jointly with Pt(6) and Pt(8) on a lower scale. In this stage, the charge on the central N(10) atom is almost null. The remnant negative charge in the cluster for this case is possibly the cause of the double barrier found for this reaction pathway. The double barrier may also be a consequence of 7-2 involving an

atom lying on the CSP mirror. For both pathways B57 and B72, the charge goes to the anti-bonding molecular orbital of N_2O , producing the weakening of the N–O bond and the consequent dissociation.

Lastly, on 8-5, the Pt(8) atom has a preponderant role in the charge transfer by activating the complex without going through the bridge formation; see Figure 8c. In fact, with large negative charge ($-0.055e$) in the bare cluster, Pt(8) appears now with a positive charge in the TS1^\ddagger stage. In a lower proportion, the Pt(5) atom also donates charge to N_2O . On this reaction pathway, via *atop* mode, the N_2O molecule seats first on the Pt(8) site with a positive net charge ($0.021e$). Note that in this stage the Hirshfeld charges on the cluster preserve the mirror symmetry (see Table S4). In the next stage, when N_2O rotates toward the Pt(5) site, the mirror symmetry is broken. Then, in the TS1^\ddagger stage (frustrated bridge), the cluster charge on the Pt(5) side of the mirror is positive, $q(\text{Pt}(5)) + q(\text{Pt}(7)) = 0.026e$, while on the other side it is negative, $q(\text{Pt}(3)) + q(\text{Pt}(6)) = -0.018e$, showing that both Pt(5) and Pt(7) donate negative charge to N_2O . Globally, the Pt_8 cluster donates negative charge to the molecule, which acquires a net charge of $-0.117e$. After this transition stage, the bridge is trying to form. However, the subtle balance of charges and forces in the $\text{Pt}_8\text{--N}_2\text{O}$ complex is not given to have equilibrium for the bridge. Even so, the charge transferred to the N_2O molecules becomes enough to reduce it spontaneously. During this reaction transition, the cluster is relaxed, elongating the Pt(8)–Pt(5) bond distance to 3.16 Å. The Pt_8 cluster is positively charged ($0.031e$) after the N_2O dissociation, and most of the positive charge ($0.194e$) is on the Pt(5) site bound with the O atom.

In summary, the transferred charge from the Pt_8 cluster to the N_2O molecule is such that it weakens the bond between the central nitrogen and the O atom, being capable of producing the N_2O reduction. Besides, if the bridge formation is attempted through Pt atoms lying on the CSP, an adequate distribution of charges is not possible, producing either desorption or dissociation without bridge formation in these routes. A question that remains open is whether the ionized states of Pt_8 could improve the catalytic efficiency, given the critical role played by the charge-transfer process. To answer this question, it is mandatory to find the new GS in those states of charge since, as we mentioned in section 3.1, there are a plethora of isomers in competition.

3.5. Conclusions. The DFT ZORA relativistic calculations performed in this work allow the characterization of the complex reduction reaction of N_2O on the surface of the low-symmetry Pt_8 cluster, which presents strong anisotropy. From the various isomeric structures that Pt_8 can assume, a triple tetragonal pyramid in a triplet spin state was determined as the ground state and selected in this work to study the reaction with the N_2O molecule. We found that multiple reaction pathways are possible for the N_2O rupture on this isomer, which are regioselective. Once the N_2O molecule is adsorbed on the cluster surface in *atop* configuration (N-bound), there is a dependence of the reaction barrier on the orientation to which the molecule is rotated to form the *bridge*. It is not possible to form a *bridge* between atoms lying on the cluster symmetry plane, including the case between the tip Pt(8) and its neighbor atoms. For this reason precisely, Pt(8) is the hot site for reduction, yielding spontaneous dissociation of N_2O from a frustrated bridge transition structure. Moreover, the ability of Pt_8 for the transference of charge, mainly via the pivot

Pt(8) site, into the antibonding molecular orbital of N_2O promotes the reduction. Remarkably, the results reveal a great fluxionality of Pt_8 , through important rearrangements that the metal cluster performs to adsorb, activate, and finally reduce the N_2O molecule. Thus, the considerable lengthening of the bond lengths of the Pt–Pt atoms forming the bridge and the weakening of the metal bonding takes place without compromising the stability of the whole cluster. Fluxionality and multiple reaction pathways appearing on the Pt_8 surface make favorable the catalytic reduction of N_2O by this cluster with low barrier energies, comparable to those of the more symmetric neutral and charged rhodium clusters: Rh_6 , Rh_6^+ , and Rh_6^- . The performed Hirshfeld population analysis shows that the transfer of charge from the cluster to N_2O weakens its N–O bond, promoting the dissociation. It was confirmed in this work that the Pt_8 particle is an efficient catalyst to reduce one N_2O molecule. However, it is important to find the reasons why this catalytic activity decreases significantly for the next molecules; we have research in progress that addresses this problem. The fact that experimental techniques as IR-MPD, implemented recently,²⁷ can be employed to model catalysts of the platinum group metal clusters makes us think that the present study can be verified in the short term.

■ ASSOCIATED CONTENT

Supporting Information

The Supporting Information is available free of charge on the ACS Publications website at DOI: 10.1021/acs.jpca.7b11055.

Optimized *atop* adsorption configurations of the N_2O molecule on the different nonequivalent sites of Pt_8 cluster (Figure S1); transition structures (TS1), *bridge* local minima, and transition structures (TS2) for the reaction pathways starting from the sites 5 (Figure S2), 7 (Figure S3), and 2 and 4 (Figure S4); transition structures (TS1) prior to spontaneous dissociation (Figure S5); and Hirshfeld charges of the complex $\text{Pt}_8 + \text{N}_2\text{O}$ as a function of the reaction stage corresponding to the B57 (Table S1), B72 (Table S2), and B85 (Table S3) reaction pathways (PDF)

■ AUTHOR INFORMATION

Corresponding Author

*Phone: 52-55-56-22-37-83. Fax: 52-55-56-16-20-10. E-mail: miguel.castro.m@gmail.com.

ORCID

Alan Miralrio: 0000-0002-7992-3718

Miguel Castro: 0000-0001-8188-7835

Notes

The authors declare no competing financial interest.

■ ACKNOWLEDGMENTS

V.B. gratefully acknowledges the financial sources provided by UAM for the access to the software used in the present work. M.C. acknowledges financial support provided by DGAPA-UNAM, under Project PAPIIT IN-212315, and from Facultad de Química, under the PAIP-FQ program. M.C. and J.S. are thankful to the Dirección General de Cómputo y de Tecnologías de la Información (DGTIC-UNAM) for providing supercomputing resources on the Miztli supercomputer (Projects LANCAD-UNAM-DGTIC-063 and LANCAD-UNAM-DGTIC-159).

REFERENCES

- (1) Smith, K. A. *Nitrous Oxide and Climate Change*; Earthscan: London, 2010; pp 1–3.
- (2) Molina, M. J.; Rowland, F. S. Stratospheric Sink for Chlorofluoromethanes: Chlorine Atom-Catalysed Destruction of Ozone. *Nature* **1974**, *249*, 810–812.
- (3) Liu, X.; Bauer, M.; Bertagnolli, H.; Roduner, E.; van Slageren, J.; Philipp, F. Structure and Magnetization of Small Monodisperse Platinum Clusters. *Phys. Rev. Lett.* **2006**, *97*, 253401.
- (4) Bartolomé, J.; Bartolomé, F.; García, L. M.; Roduner, E.; Akdogan, Y.; Wilhelm, F.; Rogalev, A. Magnetization of Pt₁₃ Clusters Supported in a NaY Zeolite: A XANES and XMCD Study. *Phys. Rev. B: Condens. Matter Mater. Phys.* **2009**, *80*, 014404.
- (5) Bunău, O.; Bartolomé, J.; Bartolomé, F.; García, L.-M. Large Orbital Magnetic Moment in Pt₁₃ Clusters. *J. Phys.: Condens. Matter* **2014**, *26* (19), 196006.
- (6) Zhai, H.; Alexandrova, A. N. Fluxionality of Catalytic Clusters: When It Matters and How to Address It. *ACS Catal.* **2017**, *7* (3), 1905–1911.
- (7) Sebetci, A.; Güvenç, Z. B. Energetics and Structures of Small Clusters: Pt_N, N = 2–21. *Surf. Sci.* **2003**, *525*, 66–84.
- (8) Xiao, L.; Wang, L. Structures of Platinum Clusters: Planar or Spherical? *J. Phys. Chem. A* **2004**, *108*, 8605–8614.
- (9) Huda, M. N.; Niranjana, M. K.; Sahu, B. R.; Kleinman, L. Effect of Spin-Orbit Coupling on Small Platinum Nanoclusters. *Phys. Rev. A: At., Mol., Opt. Phys.* **2006**, *73*, 053201.
- (10) Nie, A.; Wu, J.; Zhou, C.; Yao, S.; Luo, C.; Forrey, R. C.; Cheng, H. Structural Evolution of Subnano Platinum Clusters. *Int. J. Quantum Chem.* **2007**, *107*, 219–224.
- (11) Bhattacharyya, K.; Majumder, C. Growth Pattern and Bonding Trends in Pt_n (N = 2–13) Clusters: Theoretical Investigation Based on First Principle Calculations. *Chem. Phys. Lett.* **2007**, *446*, 374–379.
- (12) Kumar, V.; Kawazoe, Y. Evolution of Atomic and Electronic Structure of Pt Clusters: Planar, Layered, Pyramidal, Cage, Cubic, and Octahedral Growth. *Phys. Rev. B: Condens. Matter Mater. Phys.* **2008**, *77*, 205418.
- (13) Wang, X.; Tian, D. Structures and Structural Evolution of Pt_n (n = 15–24) Clusters with Combined Density Functional and Genetic Algorithm Methods. *Comput. Mater. Sci.* **2009**, *46*, 239–244.
- (14) Sebetci, A. Does Spin-orbit Coupling Effect Favor Planar Structures for Small Platinum Clusters? *Phys. Chem. Chem. Phys.* **2009**, *11*, 921–925.
- (15) Błoński, P.; Dennler, S.; Hafner, J. Strong Spin-orbit Effects in Small Pt Clusters: Geometric Structure, Magnetic Isomers and Anisotropy. *J. Chem. Phys.* **2011**, *134*, 034107.
- (16) Heredia, C. L.; Ferraresi-Curotto, V.; López, M. B. Characterization of Pt_n (N = 2–12) Clusters through Global Reactivity Descriptors and Vibrational Spectroscopy, a Theoretical Study. *Comput. Mater. Sci.* **2012**, *53*, 18–24.
- (17) Sebetci, A. New Minima for the Pt₈ Cluster. *Comput. Mater. Sci.* **2013**, *78*, 9–11.
- (18) Hamad, B.; El-Bayyari, Z.; Marashdeh, A. Investigation of the Stability of Platinum Clusters and the Adsorption of Nitrogen Monoxide: First Principles Calculations. *Chem. Phys.* **2014**, *443*, 26–32.
- (19) Chaves, A. S.; Rondina, G. G.; Piotrowski, M. J.; Tereshchuk, P.; Da Silva, J. L. F. The Role of Charge States in the Atomic Structure of Cu_n and Pt_n (n = 2–14 Atoms) Clusters: A DFT Investigation. *J. Phys. Chem. A* **2014**, *118*, 10813–10821.
- (20) Zhai, H.; Ha, M.-A.; Alexandrova, A. N. AFFCK: Adaptive Force-Field-Assisted *Ab Initio* Coalescence Kick Method for Global Minimum Search. *J. Chem. Theory Comput.* **2015**, *11*, 2385–2393.
- (21) Li, R.; Odunlami, M.; Carbonnière, P. Low-Lying Pt_n Cluster Structures (n = 6–10) from Global Optimizations Based on DFT Potential Energy Surfaces: Sensitivity of the Chemical Ordering with the Functional. *Comput. Theor. Chem.* **2017**, *1107*, 136–141.
- (22) Yamamoto, H.; Miyajima, K.; Yasuike, T.; Mafuné, F. Reactions of Neutral Platinum Clusters with N₂O and CO. *J. Phys. Chem. A* **2013**, *117*, 12175–12183.
- (23) Balteanu, I.; Petru Balaj, O.; Beyer, M. K.; Bondybey, V. E. Reactions of Platinum Clusters ¹⁹⁵Pt_n[±], n = 1–24, with N₂O Studied with Isotopically Enriched Platinum. *Phys. Chem. Chem. Phys.* **2004**, *6*, 2910–2913.
- (24) Balaj, O. P.; Balteanu, I.; Roßteuscher, T. T. J.; Beyer, M. K.; Bondybey, V. E. Catalytic Oxidation of CO with N₂O on Gas-Phase Platinum Clusters. *Angew. Chem., Int. Ed.* **2004**, *43*, 6519–6522.
- (25) Kim, M. H.; Ebner, J. R.; Friedman, R. M.; Vannice, M. A. Dissociative N₂O Adsorption on Supported Pt. *J. Catal.* **2001**, *204*, 348–357.
- (26) Bourges, P.; Lunati, S.; Mabilon, G. N₂O and NO₂ Formation during NO Reduction on Precious Metal Catalysts, Studies in Surface Science and Catalysis 116; Elsevier: Amsterdam, 1998; pp 213–222.
- (27) Harding, D. J.; Fielicke, A. Platinum Group Metal Clusters: From Gas-Phase Structures and Reactivities towards Model Catalysts. *Chem. - Eur. J.* **2014**, *20*, 3258–3267.
- (28) te Velde, G.; Bickelhaupt, F. M.; Baerends, E. J.; Fonseca Guerra, C.; van Gisbergen, S. J. A.; Snijders, J. G.; Ziegler, T. Chemistry with ADF. *J. Comput. Chem.* **2001**, *22*, 931–967.
- (29) Perdew, J. P.; Burke, K.; Ernzerhof, M. Generalized Gradient Approximation Made Simple. *Phys. Rev. Lett.* **1996**, *77*, 3865–3868.
- (30) van Lenthe, E.; Baerends, E. J.; Snijders, J. G. Relativistic Regular Two-component Hamiltonians. *J. Chem. Phys.* **1993**, *99*, 4597–4610.
- (31) van Lenthe, E.; Baerends, E. J.; Snijders, J. G. Relativistic Total Energy Using Regular Approximations. *J. Chem. Phys.* **1994**, *101*, 9783–9792.
- (32) van Lenthe, E.; Ehlers, A.; Baerends, E.-J. Geometry Optimizations in the Zero Order Regular Approximation for Relativistic Effects. *J. Chem. Phys.* **1999**, *110*, 8943–8953.
- (33) Francisco, H.; Bertin, V.; Soto, J. R.; Castro, M. Charge and Geometrical Effects on the Catalytic N₂O Reduction by Rh₆⁺ and Rh₆⁺ Clusters. *J. Phys. Chem. C* **2016**, *120*, 23648–23659.
- (34) Francisco, H.; Bertin, V.; Agacino, E.; Poulain, E.; Castro, M. Dissociation of N₂O Promoted by Rh₆ Clusters. A ZORA/DFT/PBE Study. *J. Mol. Catal. A: Chem.* **2015**, *406*, 238–250.
- (35) Kittel, C. *Introduction to Solid State Physics*, 7th ed.; John Wiley & Sons: New York, 1996.
- (36) Watanabe, Y.; Wu, X.; Hirata, H.; Isomura, N. Size-Dependent Catalytic Activity and Geometries of Size-Selected Pt Clusters on TiO₂(110) Surfaces. *Catal. Sci. Technol.* **2011**, *1*, 1490.
- (37) Beniya, A.; Isomura, N.; Hirata, H.; Watanabe, Y. Morphology and Chemical States of Size-Selected Pt_n Clusters on an Aluminium Oxide Film on NiAl(110). *Phys. Chem. Chem. Phys.* **2014**, *16*, 26485–26492.
- (38) Imaoka, T.; Akanuma, Y.; Haruta, N.; Tsuchiya, S.; Ishihara, K.; Okayasu, T.; Chun, W. J.; Takahashi, M.; Yamamoto, K. Platinum Clusters with Precise Numbers of Atoms for Preparative-Scale Catalysis. *Nat. Commun.* **2017**, *8*, 688.
- (39) Pontius, N.; Bechthold, P.; Neeb, M.; Eberhardt, W. Femtosecond Multi-Photon Photoemission of Small Transition Metal Cluster Anions. *J. Electron Spectrosc. Relat. Phenom.* **2000**, *106*, 107–116.
- (40) Roy, H. V.; Boschung, J.; Fayet, P.; Patthey, F.; Schneider, W. D. Photoemission Study of the Electronic Structure of Size-Selected Transition Metal Clusters Deposited on Ag(110). *Nanostruct. Mater.* **1993**, *2*, 163–167.
- (41) Cox, D. M.; Kaldor, A.; Fayet, P.; Eberhardt, W.; Brickman, R.; Sherwood, R.; Fu, Z.; Sondericher, D. Effect of Cluster Size on Chemical and Electronic Properties. In *Novel Materials in Heterogeneous Catalysis*; Baker, R. T. K., Murrell, L. L., Eds.; American Chemical Society: Washington, DC, 1990; Vol. 437, pp 172–187.
- (42) Plyler, E. K.; Barker, E. F. The Infrared Spectrum and the Molecular Configuration of N₂O. *Phys. Rev.* **1931**, *38*, 1827–1836.
- (43) Endou, A.; Yamauchi, R.; Kubo, M.; Stirling, A.; Miyamoto, A. Adsorption of NO on Rhodium and Palladium Clusters: A Density Functional Study. *Appl. Surf. Sci.* **1997**, *119*, 318–320.

- (44) Miralrio, A.; Sansores, L. E. Electronic Structure and Stability of Binary and Ternary Aluminum-Bismuth-Nitrogen Nanoclusters. *Int. J. Quantum Chem.* **2014**, *114*, 931–942.
- (45) Wei, X.; Yang, X. F.; Wang, A. Q.; Li, L.; Liu, X. Y.; Zhang, T.; Mou, C. Y.; Li, J. Bimetallic Au–Pd Alloy Catalysts for N₂O Decomposition: Effects of Surface Structures on Catalytic Activity. *J. Phys. Chem. C* **2012**, *116*, 6222–6232.
- (46) Xie, H.; Yang, L.; Ye, X.; Cao, Z. Mechanism of Carbon Monoxide Induced N–N Bond Cleavage of Nitrous Oxide Mediated by Molybdenum Complexes: A DFT Study. *Organometallics* **2014**, *33*, 1553–1562.
- (47) Parry, I. S.; Kartouzian, A.; Hamilton, S. M.; Balaj, O. P.; Beyer, M. K.; Mackenzie, S. R. Collisional Activation of N₂O Decomposition and CO Oxidation Reactions on Isolated Rhodium Clusters. *J. Phys. Chem. A* **2013**, *117*, 8855–8863.
- (48) Zeigarnik, A. V. Adsorption and Reactions of N₂O on Transition Metal Surfaces. *Kinet. Catal.* **2003**, *44*, 233–246.
- (49) Hermes, A. C.; Hamilton, S. M.; Hopkins, W. S.; Harding, D. J.; Kerpál, C.; Meijer, G.; Fielicke, A.; Mackenzie, S. R. Effects of Coadsorbed Oxygen on the Infrared Driven Decomposition of N₂O on Isolated Rh₃⁺ Clusters. *J. Phys. Chem. Lett.* **2011**, *2*, 3053–3057.
- (50) Hamilton, S. M.; Hopkins, W. S.; Harding, D. J.; Walsh, T. R.; Gruene, P.; Haertelt, M.; Fielicke, A.; Meijer, G.; Mackenzie, S. R. Infrared Induced Reactivity on the Surface of Isolated Size-Selected Clusters: Dissociation of N₂O on Rhodium Clusters. *J. Am. Chem. Soc.* **2010**, *132*, 1448–1449.
- (51) Chen, H.; Yue, J.; Li, Y.; Yi, C.; Yang, B.; Qi, S. Catalytic Activity Prediction of Different Metal Surfaces for N₂O Catalytic Decomposition by Density Functional Theory. *Comput. Theor. Chem.* **2015**, *1057*, 1–6.
- (52) Watanabe, K.; Kokalj, A.; Horino, H.; Rzeznicka, I. I.; Takahashi, K.; Nishi, N.; Matsushima, T. Scanning-Tunneling Microscopy, Near-Edge X-Ray-Absorption Fine Structure, and Density-Functional Theory Studies of N₂O Orientation on Pd(110). *Jpn. J. Appl. Phys.* **2006**, *45*, 2290–2294.
- (53) Andino, J. G.; Caulton, K. G. Mechanism of N/O Bond Scission of N₂O by an Unsaturated Rhodium Transient. *J. Am. Chem. Soc.* **2011**, *133*, 12576–12583.
- (54) Nguyen, H. M. T.; Pham, N. T. T. Theoretical Study on the Reaction Mechanism of N₂O with H₂ Catalyzed by the Rh₅ Cluster. *J. Phys. Chem. C* **2014**, *118*, 28562–28571.
- (55) Kokalj, A.; Matsushima, T. A Density-Functional Theory Study of the Interaction of N₂O with Rh(110). *J. Chem. Phys.* **2005**, *122*, 034708.
- (56) Matsushima, T.; Kokalj, A. Angular Distributions of Desorbing N₂ in Thermal N₂O Decomposition on Rh(100). *Surf. Sci.* **2007**, *601*, 3996–4000.
- (57) Hamilton, S. M.; Hopkins, W. S.; Harding, D. J.; Walsh, T. R.; Haertelt, M.; Kerpál, C.; Gruene, P.; Meijer, G.; Fielicke, A.; Mackenzie, S. R. Infrared-Induced Reactivity of N₂O on Small Gas-Phase Rhodium Clusters. *J. Phys. Chem. A* **2011**, *115* (12), 2489–2497.
- (58) Kerpál, C.; Harding, D. J.; Hermes, A. C.; Meijer, G.; Mackenzie, S. R.; Fielicke, A. Structures of Platinum Oxide Clusters in the Gas Phase. *J. Phys. Chem. A* **2013**, *117*, 1233–1239.